

PROCEEDINGS OF SPIE

[SPIDigitalLibrary.org/conference-proceedings-of-spie](https://spiedigitallibrary.org/conference-proceedings-of-spie)

Femtosecond pump-probe study of negative electron affinity GaAs/AlGaAs photocathodes

Hemang Jani, Liang Chen, Lingze Duan

Hemang Jani, Liang Chen, Lingze Duan, "Femtosecond pump-probe study of negative electron affinity GaAs/AlGaAs photocathodes," Proc. SPIE 10530, Ultrafast Phenomena and Nanophotonics XXII, 105300X (22 February 2018); doi: 10.1117/12.2291653

SPIE.

Event: SPIE OPTO, 2018, San Francisco, California, United States

Femtosecond pump-probe study of negative electron affinity GaAs/AlGaAs photocathodes

Hemang Jani^{*a}, Liang Chen^b, and Lingze Duan^a

^aDept. of Physics, Univ. of Alabama in Huntsville, 301 Sparkman Dr., Huntsville, AL USA 35899;

^bInstitute of Optical & Electronic Technology, China Jiliang University, 258 Xue Yuan Road, Hangzhou, Zhejiang Province 310018, P. R. China

ABSTRACT

Negative electron affinity (NEA) photocathodes have attracted a lot of interest over the last two decades due to their high quantum efficiency and low dark emission, which are desirable for night vision and other low-light applications. Recently, gradient-doping technique has shown promise to significantly improve the quantum yield of GaAs/AlGaAs heterojunction photocathodes by assisting electron diffusion toward the surface. In the present work, femtosecond pump-probe transient reflectivity measurement has been used to study the ultrafast carrier dynamics in NEA GaAs/AlGaAs photocathodes. The research focuses on the comparison between a traditional, uniform-doped structure (1.7 μm *p*-GaAs ($1 \times 10^{19} \text{ cm}^{-3}$) / 0.7 μm *p*-Al_{0.57}Ga_{0.43}As ($3 \times 10^{18} \text{ cm}^{-3}$) / si-GaAs substrate) and a gradient-doped structure (0.1 μm *p*-GaAs ($1 \times 10^{18} \text{ cm}^{-3}$) / 1.2 μm *p*-Al_{0.63}Ga_{0.37}As (doping level gradually changes from $1 \times 10^{18} \text{ cm}^{-3}$ to $1 \times 10^{19} \text{ cm}^{-3}$) / 0.5 μm *p*-GaAlAs ($1 \times 10^{19} \text{ cm}^{-3}$) / si-GaAs substrate). Our result indicates that gradient doping not only leads to more efficient electron transportation but also results in better electron accumulation (i.e. higher concentration and longer lifetime) near device surface, a feature well-suited for photocathodes. Moreover, we have shown that pump-probe transient reflectivity measurement is able to offer a direct picture of electron diffusion inside NEA photocathodes, which can be of significant importance to device development.

Keywords: Photocathodes, negative electron affinity, GaAs/AlGaAs, ultrafast effects, pump-probe, time resolved, gradient doping, transient response

1. INTRODUCTION

Negative electron affinity (NEA) semiconductor photocathodes have attracted a lot of interest over the last two decades due to their high quantum efficiency and low dark emission, which are desirable for night vision and other low-light applications¹⁻⁹. Various approaches have been explored to enhance the performances of NEA photocathodes. For example, gradient (or exponential) doping is developed to balance the requirements for long electron diffusion lengths and narrow surface band bending regions²⁻⁶. GaAs/AlGaAs heterojunction structures are used to confine carriers and to improve the flexibility of band gap selection^{7,8}. The majority of the studies on GaAs/AlGaAs NEA photocathodes so far focus on steady-state characterization, where the photocathodes are under the excitation of continuous-wave (CW) light sources such as halogen lamps^{6,9}. Transient properties of these photocathodes, on the other hand, have not received sufficient attention. Yet, temporal response of such devices under ultrafast excitation may carry important information about carrier dynamics inside the active layers. Understanding such dynamics not only leads insight into the underlying physics but also helps device designers optimize various parameters.

Here, we report our recent attempt to study ultrafast transient carrier dynamics in reflection-mode GaAs/AlGaAs NEA photocathodes by means of femtosecond time-resolved measurement. Our experiment is based on a broadband, few-cycle pump-probe system operating in the 800-nm wavelength range. By comparing the transient responses of different device structures, we show that ultrafast carrier dynamics is strongly influenced by structural configurations as well as doping profiles.

*hj0004@uah.edu; phone 1 256 824-2138; fax 1 256 824-5783; www.uah.edu/puls

Ultrafast Phenomena and Nanophotonics XXII, edited by Markus Betz, Abdulhakem Y. Elezzabi, Proc. of SPIE Vol. 10530, 105300X · © 2018 SPIE
CCC code: 0277-786X/18/\$18 · doi: 10.1117/12.2291653

Proc. of SPIE Vol. 10530 105300X-1

2. BROADBAND FEW-CYCLE PUMP-PROBE SYSTEM

2.1 System description

GaAs photocathodes are broadband devices typically operating between 500–900 nm, where they reach peak quantum yields^{1,2}. When studying such devices, it is ideal to use broadband ultrafast light sources with as much spectral overlap as possible to the device operating wavelength range. In the current research, a few-cycle pump-probe transient reflectivity (PPTR) system with about 300-nm spectral coverage has been developed. Figure 1 shows the schematics of the PPTR system. A sub-8-fs Ti:Sapphire laser (Venteon Pulse:One PE) serves as the light source. It is able to generate 540-mW average power at an 83-MHz repetition rate. In order to preserve the few-cycle pulses during pulse transportation, care must be taken to manage the dispersion in the transportation path. First, material dispersion is minimized by employing an all-reflective beam path, which includes a periscope (PR1 and PR2) for generating a cross-polarized probe beam. Second, a dispersion-balanced broadband beamsplitter (BS1) is used to split the pump and the probe beams with about the same amount of dispersion in both arms. Finally, a dispersion-compensating mirror (DCM) pair and a CaF₂ wedge pair are utilized to balance the dispersion caused by the air path and all the optics. The pump beam has about 270 mW of average power and is focused on the sample near the normal direction. A mechanical chopper chops the pump beam at 1.8 kHz. The probe beam has an average power of about 20 mW and is focused onto the sample at approximately 15°, with a focusing area smaller than the pump. The reflected probe passes through a polarizer to remove scattered pump before impinging on a photodetector. The detector output feeds into a lock-in amplifier (SRS SR830), which selectively amplifies the change of the reflected probe power due to the pump pulses. A motorized translation stage (Newport VP-25XA) in the pump arm scans the relative delays between the pump pulses and the probe pulses.

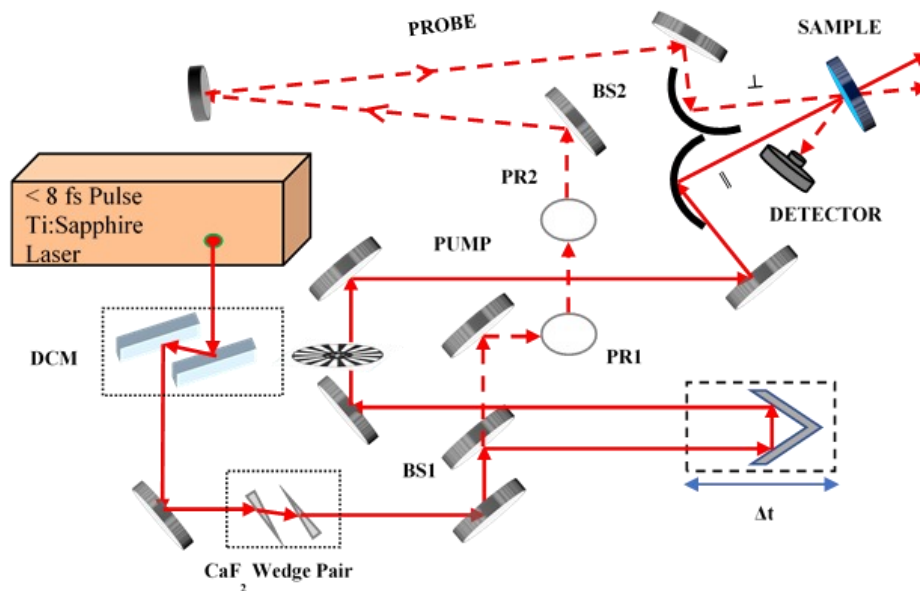


Figure 1. Layout of the broadband pump-probe system. BS: beamsplitter; DCM: dispersion-compensating mirror; PR: periscope; // and ⊥ indicate polarization states.

2.2 Characterization and calibration

The pump pulse is characterized at the location of the sample with spectral phase interferometry using direct electric field reconstruction (SPIDER) and both the time-domain and the frequency-domain results are shown in Figure 2. A full-width-at-half-maximum (FWHM) duration of 6.5 fs is obtained with the time-domain measurement (Figure 2(a)) and a 300-nm spectral coverage at 20 dB below the peak can be seen in the frequency-domain trace (Figure 2(b)). The probe pulse is estimated to be sub-10 fs as well. Both beams are focused on the sample using off-axis parabolas and their spatial overlap is optimized using a laser beam profiler. In addition to the ac output of the photodetector, which is amplified by the lock-in amplifier, the dc output current of the detector is also monitored with an oscilloscope. This

allows for the calibration of the overall probe power incident on the detector, which in turn is used to calibrate the relative reflectivity change of the sample due to pump pulse-induced carrier dynamics^{10,11}.

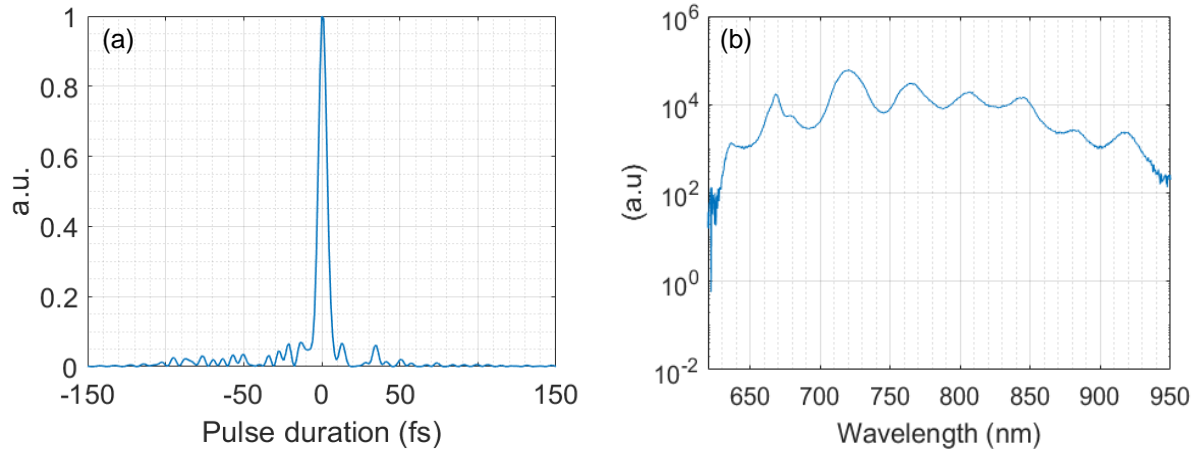


Figure 2. SPIDER characterization of the few-cycle pulses. (a) Time-domain trace shows a 6.5 fs FWHM duration for the pump pulses. (b) Spectrum of the laser shows a 300-nm spectral coverage.

3. EXPERIMENTAL RESULTS

3.1 PPTR measurement of GaAs sample

In order to verify the effectiveness of our PPTR system, we first take measurement using a GaAs substrate as the sample. The substrate is *p*-doped at $1 \times 10^{16} \text{ cm}^{-3}$ level, with a thickness of $370 \mu\text{m}$. The measured relative-reflectivity evolution is shown in Figure 3, where “Time” represents the relative delay between the probe and the pump pulses. This result agrees with typical PPTR behaviors for GaAs^{12,13}, where a sharp increase of reflectivity is followed by an exponential decay. The comparably longer carrier lifetime ($\sim 20 \text{ ps}$) in the current case is believed to be due to the use of a GaAs substrate, which has a much lower concentration of defects than epitaxial GaAs. The result demonstrates the capability of our PPTR system in studying transient carrier dynamics in semiconductor devices.

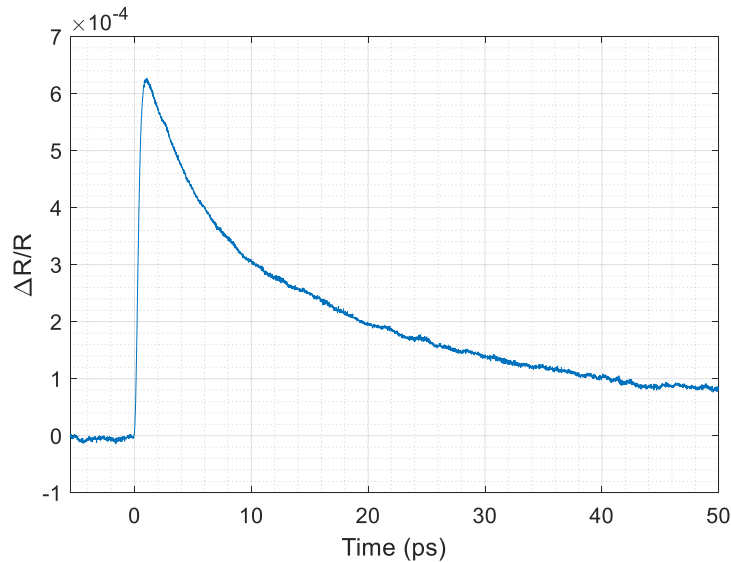


Figure 3. PPTR trace measured with a GaAs substrate ($1 \times 10^{16} \text{ cm}^{-3}$ *p*-doped).

3.2 Comparable study of GaAs/AlGaAs photocathodes

Our study of GaAs/AlGaAs photocathodes focuses on two device structures. Figure 4 shows the schematics of the two devices. Device #1 uses Si-doped GaAs (370 μm) as the substrate. A 0.7- μm layer of $p\text{-Al}_{0.57}\text{Ga}_{0.43}\text{As}$ with a doping concentration of $3 \times 10^{18} \text{ cm}^{-3}$ is directly grown on the substrate to serve as the buffer layer. Grown on top of the buffer layer is the active layer, which is 1.7 μm of $p\text{-GaAs}$ uniform-doped at $1 \times 10^{19} \text{ cm}^{-3}$. Device #2 is built upon the same substrate as Device #1, with a 0.5- μm buffer layer made of $p\text{-GaAlAs}$ doped at $1 \times 10^{19} \text{ cm}^{-3}$. The active layer is 1.2 μm of $p\text{-Al}_{0.63}\text{Ga}_{0.37}\text{As}$, gradient-doped from $1 \times 10^{19} \text{ cm}^{-3}$ (buffer layer side) to $1 \times 10^{18} \text{ cm}^{-3}$ (cap layer side). The device is capped by 0.1- μm layer of $p\text{-GaAs}$ with a doping concentration of $1 \times 10^{18} \text{ cm}^{-3}$. Both photocathodes are surface-activated by means of a Cs-O layer on the front surface.

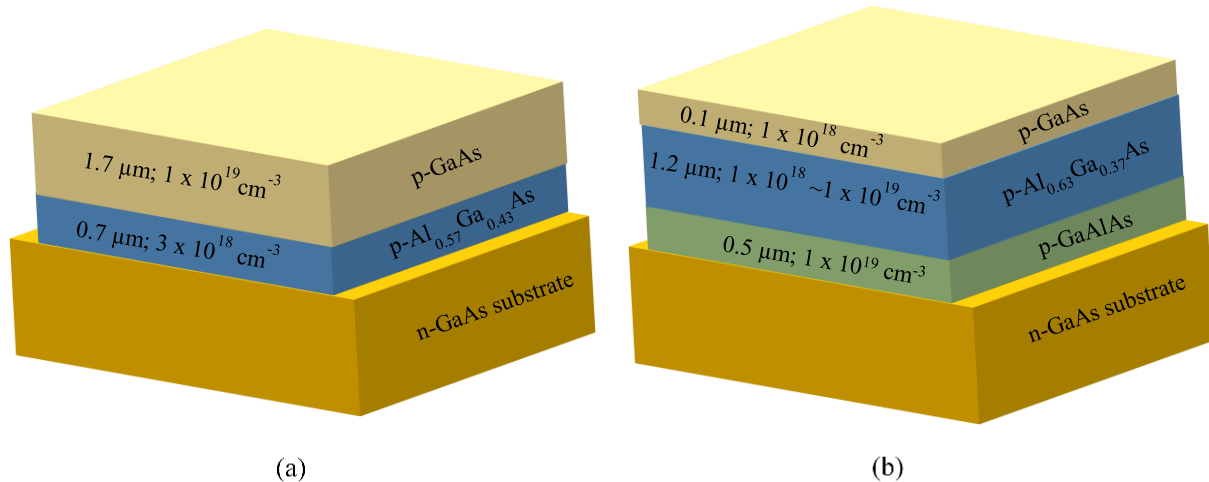


Figure 4. Doping structure diagram of the two GaAs/AlGaAs photocathodes. (a) Device #1: uniform-doped $p\text{-GaAs}$ as active layer. (b) Device #2: gradient-doped $p\text{-Al}_{0.63}\text{Ga}_{0.37}\text{As}$ as active layer.

The PPTR measurements on the two devices are performed under similar experimental conditions. Figure 5 (a) and (b) show the measured transient reflectivity responses for Device #1 and Device #2, respectively. Comparing the two traces, several similarities and differences can be drawn.

First of all, after the excitation of the pump pulse, it takes about 3 ps for the reflectivity to reach its maximum in both devices. Moreover, in both cases, the reflectivity experiences a sharp initial rise within the first picosecond following the excitation. After that, the increase gradually slows down until the reflectivity maximizes. All these behaviors suggest that there is a carrier transportation process after the pump pulse impinges onto the sample. The initial rise of the reflectivity is likely caused by the photo-generated free electrons near the surface. The electrons generated deeper inside the active layer diffuse toward the surface, causing the reflectivity to continue to rise, albeit at a gradually reducing rate. The gradient-doped sample (Device #2) achieves a higher peak value of $\Delta R/R$ (2.85×10^{-4} vs. 1.75×10^{-4}), indicating possibly more efficient carrier transportation. This is in agreement with prior reports on similar doping structures^{3,4,5}, where gradient doping is found to improve electron diffusion length.

Upon reaching their peak values, the reflectivities of both devices begin to decrease as carrier relaxation begins to dominate. However, the relaxation characteristics of the two photocathodes are markedly different. Device #1 exhibits a relatively faster relaxation (Figure 5(a)), with $\Delta R/R$ falling to less than one half of its peak value within 50 ps (maximum measurable delay). The reduction rate of $\Delta R/R$ is nearly constant, with a slight increase toward larger delays. This kind of behavior suggests that multiple processes may take place simultaneously during this period and some of them counter balance the relaxation of free electron concentration near the surface. The exact mechanism is subject to further theoretical analysis. One possible scenario is that thermalized free electrons from deeper inside the device continue to diffuse toward the surface while carrier relaxation occurs near the surface. Meanwhile, Device #2 exhibits a much slower relaxation process as shown in Figure 5(b). Extrapolation of the experimental curve shows that it would take about 300 ps for $\Delta R/R$ to fall to one half of its peak value (assuming the decay rate remains the same). This distinction between the

two photocathodes likely stems from their difference in doping structures. The gradient-doped structure in Device #2 apparently leads to stronger electron population buildup near the surface. In the meantime, the lower doping level near the surface of Device #2 results in longer carrier lifetime.

Overall, the gradient-doped structure appears to create a more favorable condition for the operation of a photocathode than the more traditional uniform-doped structure. This conclusion does not come in surprise as many reports in the past have shown the effectiveness of gradient-doping in enhancing quantum efficiency^{3,4,5}. However, the current work takes a completely different approach and makes the comparison from the perspective of transient carrier dynamics. It should be noted that the above analysis completely neglects photoelectron emission from the photocathodes. This is justified because it has been shown that the response time of NEA photocathodes is typically on nanosecond scale¹⁴, much longer than the relevant time scale in this study.

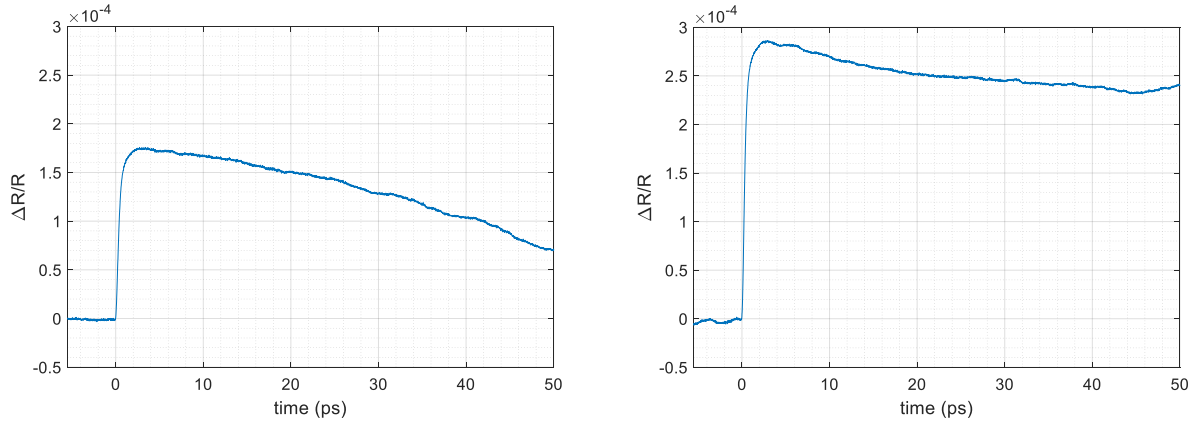


Figure 5. PPTR measurement results for NEA GaAs/AlGaAs photocathodes: (a) uniform-doped structure; (b) gradient-doped structure.

4. CONCLUSION

In conclusion, we have developed a broadband, few-cycle PPTR system and performed PPTR measurements on NEA GaAs/AlGaAs photocathodes with two different doping structures. Our result indicates that gradient doping not only leads to more efficient electron transportation but also results in better electron accumulation (i.e. higher concentration and longer lifetime) near device surface. Moreover, we have shown that femtosecond PPTR measurement is able to offer a direct picture of electron diffusion inside NEA photocathodes, something traditional dc approaches unable to provide. Future work includes more detailed theoretical modeling and theory-experiment comparisons, which will lead to deeper understanding of the carrier dynamics in such devices.

5. ACKNOWLEDGEMENT

This work was supported in part by the National Science Foundation (NSF) under Grant ECCS-1254902 and ECCS-1606836, and in part by the National Natural Science Foundation of China under Grant No. 61775203 as well as the National Key Research and Development Program of China under Grant No. 2017YFF0210800.

The authors acknowledge the key support to this research by Dr. Yunsheng Qian of Nanjing Institute of Science and Technology, China, who supplied the photocathode devices.

REFERENCES

- [1] Olsen, G. H., Szostak, D. J., Zamerowski, T.J. and Eternberg, M., "High-performance GaAs photocathodes," *J. Appl. Phys.* 48(3), 1007-1008 (1977).

- [2] Zou, J. and Chang, B., "Gradient-doping negative electron affinity GaAs photocathodes," *Opt. Eng.* 45(5), 054001 (2006).
- [3] Yang, Z., Chang, B., Zou, J., Qiao, J., Gao, P., Zeng, Y., and Li, H., "Comparison between gradient-doping GaAs photocathode and uniform-doping GaAs photocathode," *Appl. Opt.* 46(28), 7035-7039 (2007).
- [4] Niu, J., Zhang, Y., Chang, B., Yang, Z., and Xiong, Y., "Influence of exponential doping structure on the performance of GaAs photocathodes," *Appl. Opt.* 48(29), 5445-5450 (2009).
- [5] Zhang, Y., Zou, J., Niu, J., Zhao, J., and Chang, B., "Photoemission characteristics of different-structure reflection-mode GaAs photocathodes," *J. Appl. Phys.* 110(6), 063113 (2011).
- [6] Chen, X., Zhao, J., Chang, B., Yu, X., Hao, G., Xu, Y. and Cheng, H., "Photoemission characteristics of (Cs, O) activation exponential-doping $\text{Ga}_{0.37}\text{Al}_{0.63}\text{As}$ photocathodes," *J. Appl. Phys.* 113(21), 213105 (2013).
- [7] Farsakoglu, O. F., Zengin, D.M. and Kocabas, H., "Determination of some main parameters for quantum values of GaAlAs/GaAs transmission-mode photocathodes in near-infrared region," *Opt. Eng.* 32(5), 1105-1113 (1993).
- [8] Zhang, Y., Jing, Z., Jun, Z., Jun, N., Long, C. and Kang, C., "The High Quantum Efficiency of Exponential-Doping AlGaAs/GaAs Photocathodes Grown by Metalorganic Chemical Vapor Deposition," *Chin. Phys. Lett.* 30(4), 044205 (2013).
- [9] Zou, J., Chang, B., Chen, H. and Liu, L., "Variation of quantum-yield curves for GaAs photocathodes under illumination," *J. Appl. Phys.* 101(3), 033126 (2007).
- [10] Shank, C. V., Yen, R., and Hirlimann, C., "Time-resolved reflectivity measurements of femtosecond-optical-pulse-induced phase transitions in silicon," *Phys. Rev. Lett.* 50, 454 (1983).
- [11] Wolpert C., Dicken, C., Atkinson, P., Wang, L., Rastelli, A., Schmidt, O.G., Giessen, H. and Lippitz, M., "Transient reflection: a versatile technique for ultrafast spectroscopy of a single quantum dot in complex environments," *Nano Lett.* 12 (1), 453–457 (2012).
- [12] Yano, R., Hirayama, Y., Miyashita, S., Sasabu, H., Uesugi, N., and Uehara, S., "Pump-probe spectroscopy of low-temperature grown GaAs for carrier lifetime estimation: arsenic pressure dependence of carrier lifetime during MBE crystal growth," *Phys. Lett. A* 289, 93-98 (2001).
- [13] Ortiz, V., Nagle, J., Lampin, J. F., Peronne, E., and Alexandrou, A., "Low-temperature-grown GaAs: Modeling of transient reflectivity experiments," *J. Appl. Phys.* 102, 043515 (2007).
- [14] Spicer, W. E. and Herrera-Gomez, A., "Modern theory and applications of photocathodes," *Proc. SPIE* 2022, 18-33 (1993).